Towards artificial photosynthesis : resolving supramolecular packing of artificial antennae chromophores through a hybrid approach

Thomas, B.

Chapter 2

Surface-deposited DATZnS(3′-NMe) chromophore light harvesting antennae form parallel molecular stacks in an antiparallel lamellar packing framework

Abstract

The supramolecular packing of the fused napthalenediimide-zinc-salphen based light harvesting chromophore DATZnS(3′-NMe) with a molecular recognition site incorporated into a chromophoric structure and deposited on a surface grid was determined by computational integration of cryo-EM imaging and magic angle spinning (MAS) NMR with ^{1}H-^{13}C heteronuclear dipolar correlation spectroscopy and ^{13}C at natural abundance. Absence of doubling in ^{13}C spectra and calculation of molecular energy point to an intramolecular C_2 symmetry for the chiral DATZnS(3′-NMe) motif. Diffraction patterns obtained by Fourier transformation of TEM images with 0.6 nm resolution indicate a monoclinic packing with the DATZnS(3′-NMe) along the unique axis of 1.685 nm and two shorter axes of 0.547 nm and 2.517 nm under an angle of 102°. This leads to a density of 1.67 g/cm^3 with two molecules in the unit cell. Systematic absences reveal a translational component, either a screw axis or a glide plane to accommodate steric hindrance that predominantly determines the packing. The internal C_2 symmetry and the absence of doubling in the MAS NMR point to a twofold axis in either a chiral packing with two independent positions or an achiral racemic paracrystalline packing with four independent positions to accommodate the two enantiomeric forms of the salphen motif with Λ and the Δ enantiomers present in equal amounts. The only space group that fulfills the requirements is $P2/c$ with four independent positions that are both necessary and sufficient to account for the internal symmetry of the DATZnS(3′-NMe) as well as the presence of the two

enantiomeric forms. Other space groups either have more independent positions, *e.g.* eight for a racemic packing or four for a chiral packing or they require more than two molecules in the unit cell, or they do not reproduce the systematic absences in the diffraction pattern. In the structure, the molecules are in parallel stack arrangement with the phenazine dipoles head to tail. The two enantiomeric forms lead to sheets running antiparallel to form a 3D structure. The molecular recognition interaction between the salphen and the bromine leads to a pseudo-octahedral arrangement of zinc, which explains the richness in the structure with its two enantiomeric forms. The packing is confirmed by selective NMR distance constraints, between protons from the dimethyl functionalities in the salphen and NDI ring carbons adjacent to the Br, and between the alkyl chains and the phenazine core. Simulations of TEM diffraction reproduce the reflection conditions and allow determining the orientation of the lamellar morphology relative to the surface, which is important in view of the future application in artificial photosynthesis with complex supramolecular motifs bolted onto electrodes. The NDI rings are parallel to the surface, providing an interesting opportunity to make a configuration for *e.g.* injection of charge into a catalyst system.

2.1 Introduction

The world is moving towards a technological transformation, driven by the need to replace fossil fuel by renewables.[1-9] One out of very few options to achieve this is by artificial photosynthesis, which is the fine art of mimicking the processes of natural photosynthesis found in plants and some bacteria.[10-13] Biological systems are complicated with little true complexity. The biological design builds on "responsive matrices", protein complexes for light harvesting, charge separation and catalysis, which proceed with near-unity yield.[14] Any responsive matrix has an energy landscape that is determined by the structure, which on the one hand is stabilized with respect to the denatured or unfolded state, while on the other hand it is broadened by induced misfits and conformational entropy that allows for a quantum coherent functional response.[15,16] In contrast, supramolecular design often aims for tightly fitting assemblies, that leave little room for the frustration and the dynamic shaping that is necessary for steering reactivity and we have to

develop new chemical tools for engineering the packing by molecular recognition motifs, ultimately leading to functional assemblies. Here I explore how a zinc-salphen recognition motif steers the packing when fused to a naphthalene diimide chromophore to form a phenazine and deposited on a surface, a topology of interest to artificial photosynthesis applications. DATZnS(3′-NMe) is a fused NDI-zinc-salphen based chromophore that was designed with the optical and electronic properties of chlorophylls in mind and is much more robust than biological components.[17-25] Like chlorophylls, DATZnS absorbs sunlight by an extended conjugated π-system, has an electric dipole moment that can be utilized for structural and functional control, and has a divalent metal ion that does not interfere with the photochemistry.[17] It can bind with Lewis bases in the surrounding for molecular recognition and scaffolding of the packing in artificial photosynthetic systems.[26-28] Natural dyes can form functional antennae by self-scaffolding, without a protein component. In chlorosome antennae, hundreds of thousands of excitonically coupled bacteriochlorophyll natural dye molecules form the largest light antennae known in nature, capable of rapid transfer of energy over more than 100 nm.[29,30] Chlorosome structures do not depend on proteins for their structural and functional integrity and provide their own scaffolding.[31-33] They may serve as a supramolecular biological paradigm for how to perform structural design of a novel class of extended systems for artificial photosynthesis by molecular recognition and packing.[34] The key to their success is a pseudosymmetric framework where all monomeric building blocks perform the same functional role in well-ordered domains. Alternating chirality of monomers induced by the packing in stacks and sheets leads to induced misfits and conformational entropy.[15]

The aim of this study is to develop a toolbox for structural control in the chemical design of artificial light harvesting systems by packing induced self-assembly of moderately sized building blocks with isomerism. Here it is shown that it is possible to select conformers and isomers by packing and derive systematics for working with racemic paracrystalline materials. While frustration and combination of different functional motifs are necessary for a responsive and reactive chemical design, it will give rise to modulated assembly and lead to paracrystalline supramolecular arrangements. A principal challenge is then how to

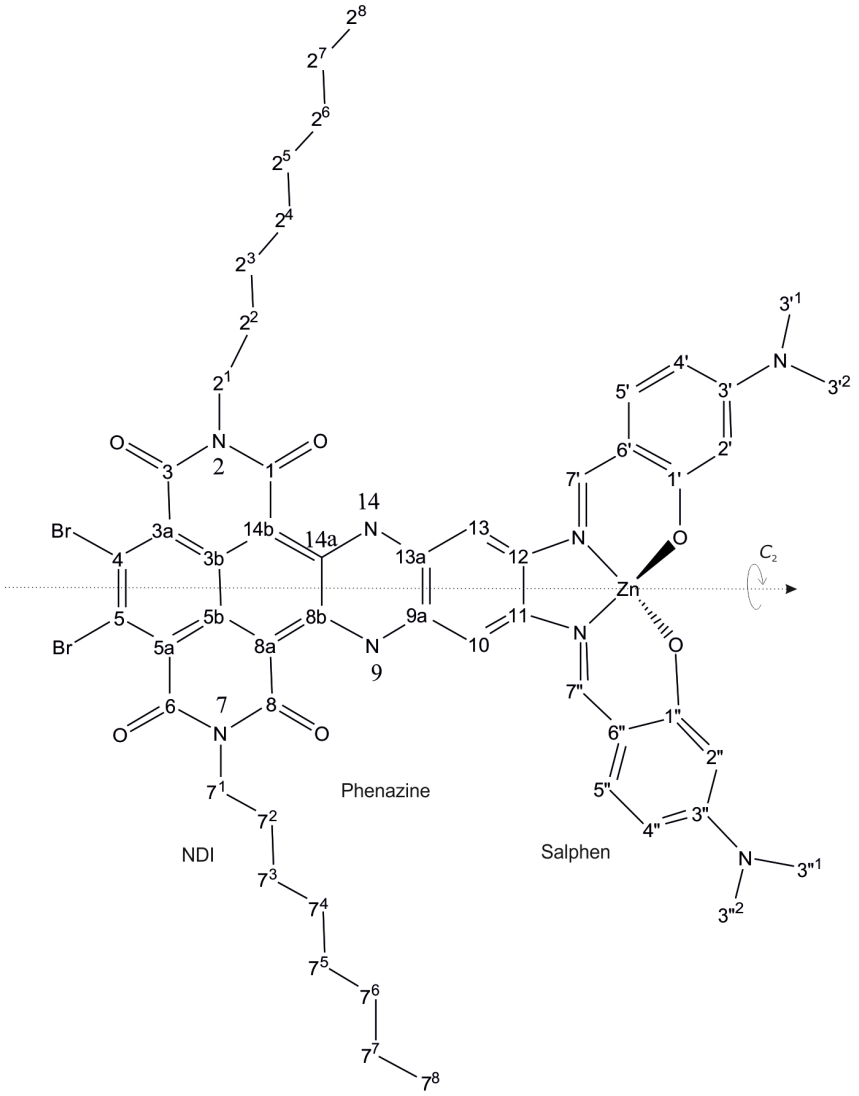

Figure 2.1 Chemical structure of the fused NDI-zinc-salphen based chromophore DATZnS(3′-NMe), a hybrid of NDI, Phenazine and Salphen with a C_2 axis of symmetry along the principal axis. The numbering is according to the IUPAC convention.

resolve the well-determined, limited true complexity from the heterogeneous background. The major challenge is to extract the functionally relevant order that is targeted by the chemical design, in a supramolecular packing that is inaccessible to high resolution X-ray and other diffraction methods for structure determination. Recently Ganapathy *et al.* have addressed this challenge by computational integration of MAS NMR and transmission electron microscopy (TEM) to resolve supramolecular packing order for a natural light collector.[35] In this approach, a library of structures is created based on reflection conditions in TEM imaging,

where the obtainable structure information in reciprocal space was a layer line along the meridian orthogonal to a strong symmetric reflection on the equator in the 2D diffraction pattern.[35] A model for the packing was refined with the help of chemical shifts and a few intermolecular correlation peaks obtained from homonuclear correlation spectroscopy done by proton spin diffusion and ^{1}H-^{13}C heteronuclear correlation data collected at a mixing time of 4 ms.[35] While the previous work concentrated on layer lines to guide the modeling of a helical structure on a cylinder, here I took the next step to resolve the packing for the DATZnS(3′-NMe) dye (Figure2.1), when forming a lamellar morphology on a surface, a technologically demanding configuration of strong relevance to possible future application in electrodes for artificial photosynthesis. I use the symmetry, repeats and reflection conditions obtained from Fourier transforms of TEM images of samples deposited on carbon grids to estimate the unit cell parameters and to identify symmetry operators with a translational component, *i.e.* a screw axis or glide plane. A 3D model for the packing was prepared with Materials studio and validated by simulation of the Fourier transform of the electron diffraction pattern. In addition, distance constraints were extracted from heteronuclear dipolar correlation data by simulating LGCP build up curves to measure ^{1}H-^{13}C distances for selected nuclei. Finally, the preferred orientation of DATZnS(3′-NMe) lamellae on the surface was determined by simulation of the TEM diffraction pattern from a supercell of DATZnS(3′-NMe). The methodology discussed here can be extended to other unlabeled samples for which it is difficult to find packing by more conventional methods.

2.2 Results

2.2.1 Chemical shift assignment and HETCOR analysis

DATZnS(3′-NMe) is a moderately sized molecule with extensive functionalities, arising from fusing functionalized NDI with functionalized salphen and establishing a phenazine bridge. Such chemical richness may be considered intrinsic for future classes of supramolecular architectures with advanced functionality. In addition, as steering the packing with molecular recognition will inevitably give rise to steric hindrance and characteristic aggregation shifts of the

NMR response, this will further contribute to a good resolution compared to the smaller compounds that are currently the standard in NMR crystallography.[35,36] Well in line with the earlier work on self-assembled moderately sized chlorophyll, chlorin and porphyrin type systems, the 1D CP/MAS spectrum of DATZnS(3′-NMe) collected with a spinning frequency of 11 kHz reveals a very good dispersion of ^{13}C chemical shifts, extending over a range of ~170 ppm.[35] This is an essential feature for structure determination of unlabeled materials, as many ^{13}C signals are well resolved in 1D with ^{13}C at natural abundance (Figure S2.3) which are summarized in Table 2.1. The aromatic signals from the NDI cover an extended range, between 150 and 170 ppm, due to the presence of the electronegative Br and keto oxygen substituents that produce extensive downfield shifts for various carbons due to the stabilization of positive charge. Also, the nitrogens in the phenazine motif contribute to the dispersion, in a more moderate way. The 3′-NMe that hyperconjugate to the salphen ring can stabilize negative charge on selected ^{13}C positions with signals shifting upfield to ~100 ppm, in competition with the stabilization of some positive charge from the oxygens bridging to the Zn^{2+} ion. Finally, the aliphatic region of the spectrum remains crowded, with the signals from the alkyl chains at the N2 and N7.

The DATZnS(3′-NMe) and its DAT-diamine precursor (Figure S2.1) are both insoluble, and a conclusive assignment of chemical shifts in the solid state is difficult with ^{13}C at natural abundance. Therefore we perform a homology assignment based on ^{1}H-^{13}C HSQC, ^{1}H-^{1}H COSY and HMBC data collected from the related compound DATZnSTP dissolved in C_6D_6 (Table 2.2). The assignment is validated with ^{1}H-^{13}C HETCOR and NMR chemical shift calculations. A set of 2D HETCOR spectra with a short mixing time of 0.256 ms and a long mixing time of 4 ms was collected (Figure 2.2). The short contact time unambiguously reveals the carbon nuclei with directly bonded protons (Figure 2.2). Due to the good dispersion, a conclusive assignment of the five aromatic C-H signals is straightforward (Table 2.1). The 2^1, 7^1 N-CH_2 well as the 3′, 3′′ N-CH_3 provide a characteristic response around 40 ppm and the terminal CH_3 of the alkyl chain resonate most up field at ~13 ppm. None of these signals shows doubling, which provides converging and convincing evidence that the two halves of the molecule are related by symmetry. This provides convincing evidence for a symmetric

DATZnS(3′-NMe) building block, with a twofold axis or a mirror plane running along the center of the phenazine motif. A pseudo octahedral coordination of the zinc salphen motif significantly contributes to the complexity of the system and can provide a handle for steering of the structure by packing effects. The wings of the salphen can be either in the *syn* or *anti*-configuration, and for the *anti*-configuration, two enantiomeric chiral isomers exist for the zinc octahedral surrounding, the Λ and Δ pair. Optimization on the enantiomeric pairs shows that an energy minimum of 10 kcal/mol limits the structure to an *anti*-configuration. The narrow lines with a linewidth of ~1 ppm for selected signals show that the system is at least paracrystalline, as *e.g.* a semicrystalline or disordered system

Table 2.1 Experimental and calculated ^{13}C chemical shifts of the DATZnS(3′-NMe)

Position	$\sigma^{C}_{DATZnS(3'\text{-}NMe),\ expt}$	$\sigma^{C}_{DATZnS(3'\text{-}NMe),\ calc}$
4, 5	154.6, 154.6	152.5, 152.5
3a, 5a	23.8, 123.8	125.6, 125.3
3, 6	166.6, 166.6	162.9, 162.9
3b, 5b	136.9, 136.9	130.0, 130.0
14b, 8a	112.1, 112.1	101.3, 101.3
13a, 9a	123.8, 123.8	129.0, 129.0
13, 10	100.1, 100.1	99.8, 99.8
12, 11	138.1, 138.1	142.1, 142.1
7', 7"	166.6, 166.6	150.2, 150.2
6', 6"	123.8, 123.8	122.7, 122.7
5', 5"	136.9, 136.9	138.2, 138.2
3', 3"	156.7, 156.7	154.1, 154.1
4', 4"	102.1, 102.1	109.1, 109.1
2', 2"	102.1, 102.1	108.5, 108.5
1', 1"	171.7, 171.7	176.7, 176.7
2^1 ,7^1	42.4, 42.4	46.9, 46.9
2^2, 7^2	28.6, 28.6	32.3, 32.3
2^3, 7^3	28.1, 28.1	34.5, 34.5
2^4, 7^4	30.7, 30.7	36.7, 36.7
2^5, 7^5	31.8, 31.8	35.1, 35.1
2^6, 7^6	30.7, 30.7	41.8, 41.8
2^7, 7^7	23.2, 23.2	29.3, 29.4
2^8, 7^8	13.7, 13.7	17.8, 17.8
$3'^1$ $3'^2$, $3''^1$, $3''^2$	39.0, 39.0, 39.0, 39.0	43.3, 43.3, 43.4, 43.4

Table 2.2 Experimental and calculated ^{13}C chemical shifts of the DATZnSTP

Position	$\sigma^{C}_{DATZnSTP, expt}$	$\sigma^{C}_{DATZnSTP, calc}$
4, 5	140.6, 140.6	152.5, 152.5
3a, 5a	121.7,121.7	125.8,126.3
3,6	160.0,160.0	163.4,163.5
3b,5b	127.3,127.3	130.5,129.9
14b, 8a	95.5, 95.5	101.9, 102.5
1, 8	164.6, 164.6	167.0, 166.8
14a, 8b	127.5, 127.5	139.0, 138.7
13a, 9a	125.7, 125.7	129.8, 129.8
13, 10	102.9, 102.9	104.4, 102.1
12, 11	139.5, 139.5	146.8, 145.7
7', 7"	162.0, 162.0	158.4, 156.4
6', 6"	118.9, 118.9	127.7, 127.1
5', 5"	129.7, 129.7	136.5, 132.0
4', 4"	135.3, 135.3	142.6, 143.0
3', 3"	130.7, 130.7	133.1, 135.8
2', 2"	143.3, 143.3	148.8, 151.5
1', 1"	173.4, 173.4	177.5, 177.4
$4'^{1}$, $4"^{1}$	34.2, 34.2	44.4, 45.2
$4'^{2}$, $4"^{2}$	31.8, 31.8	35.3, 33.6
$4'^{3}$, $4"^{3}$	31.8, 31.8	35.1, 30.4
$4'^{4}$, $4"^{4}$	31.8, 31.8	30.8, 33.7
$2'^{1}$, $2"^{1}$	36.3, 36.3	47.7, 46.9
$2'^{2}$, $2"^{2}$	30.2, 30.2	34.6, 34.8
$2'^{3}$, $2''^{3}$	30.2, 30.2	30.5, 29.3
$2'^{4}$, $2''^{4}$	30.2, 30.2	30.1, 29.5
1''', 5'''	149.2, 149.2	149.6, 153.9
5'''	149.2	153.91
2''', 4'''	121.4, 121.4	127.8, 126.0
3'''	161.3	168.2
$3'''^{1}$	34.4	45.4
$3'''^{2}$, $3'''^{3}$, $3'''^{4}$	30.0, 30.0, 30.0	34.1, 34.4, 29.4
2^{1}, 7^{1}	41.5, 41.5	48.4, 49.1
2^{2}, 7^{2}	28.3, 28.3	33.3, 33.1
2^{3}, 7^{3}	27.8, 27.8	32.1, 31.9
2^{4}, 7^{4}	29.8, 29.8	36.6, 41.1
2^{5}, 7^{5}	29.8, 29.8	29.3, 31.6
2^{6}, 7^{6}	32.2, 32.2	37.4, 43.1
2^{7}, 7^{7}	23.1, 23.1	25.0, 32.6
2^{8}, 7^{8}	14.4, 14.4	14.6, 18.6

would give rise to pronounced susceptibility broadening of signals.[37,38] The remaining aliphatic response is associated with the CH_2 of the aliphatic tail. The quaternary carbon response is detected in the ^{1}H-^{13}C HETCOR dataset collected with long CP contact time of 4 ms. The 4, 5 ^{13}C adjacent to the Br are assigned to the response at 154.6 ppm, in line with NMR shift calculations for a C_2 symmetric monomer (Table 2.1). The ^{13}C next to the keto oxygens are shifted to 159.8 and 166.6 ppm and are in line with the solution NMR response of the homologue at 160and 164.6 ppm, for the 1, 8 ^{13}C and the 3, 6 ^{13}C, respectively. Similarly the 1', 1" ^{13}C near to the bridging oxygens in the salphen have a characteristic chemical shift of 171.7 ppm, which is in line with the shift of 173.4 ppm for the homologue in solution. Remaining assignments were obtained either by analogy with the solution chemical shifts of the related molecule DATZnSTP (Figure S2.4), or were performed by computation of chemical shifts (Table 2.2). The NMR data are in line with a molecular configuration that has a C_2 axis passing through the centers of NDI and salphen as shown in Figure 2.1.

Intermolecular correlations were obtained from heteronuclear ^{1}H-^{13}C spectra recorded with a long LGCP contact time of 4 ms (Figure 2.2).[39] Pronounced correlation signals are observed between the $3'^{1}$, $3'^{2}$, $3''^{1}$, $3''^{2}$ protons resonating with 0.6 ppm ^{1}H chemical shift on salphen and 4, 5 ^{13}C nuclei on the NDI motif and are indicated with an asterisk. These correlation signals can be attributed to long-range transfer since they are not observed in the dataset collected with a short mixing time. The nearest intramolecular ^{1}H are the 2^{1}, 7^{1} CH_2 at a distance of 4.8 Å that resonates with a different ^{1}H chemical shift of 0.4 ppm. The long range transfer between 3′-NMe and 4, 5 ^{13}C provides strong NMR evidence that molecular recognition between the NDI part of the molecule and the salphen motif of an adjacent molecule is steering the packing. In addition, long-range correlation peaks are observed between protons on the alkyl chain and 11, 12, 3b, 5b, 13a, 9a, 14b, 8a, 10, 13 ^{13}C nuclei on the phenazine backbone. These long-range correlation signals could be inter or intramolecular and provide information about the positioning of the alkyl chain in the packing.

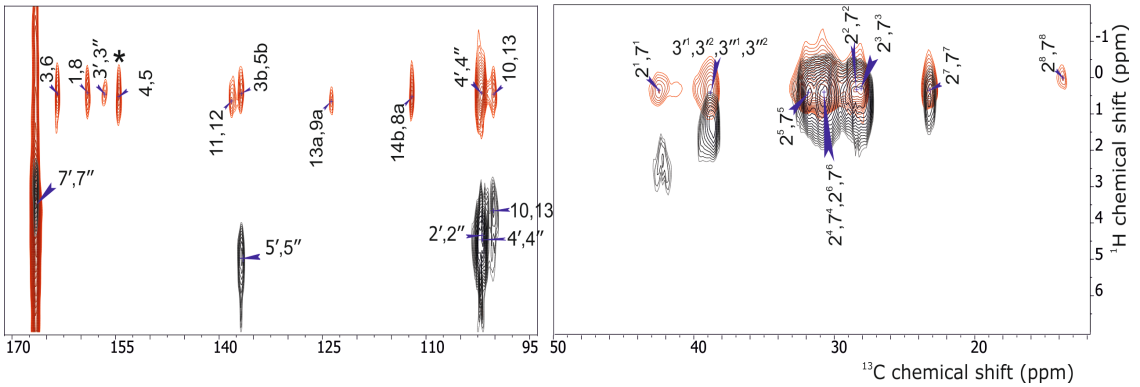

Figure 2.2 Contour plot sections of ^{1}H-^{13}C heteronuclear MAS NMR dipolar correlation spectra of DATZnS(3′-NMe) recorded in a magnetic field of 17.6 T employing a spinning rate of 11 kHz and data were collected at a sample temperature of 298 K. CP contact times of 4 ms (red) and 1 ms (black) were used to distinguish inter and intramolecular correlation peaks. The left panel shows the aromatic and carbonyl region, while the aliphatic response is shown in the right panel. Correlation peaks are indicated by numbers corresponding to the assignment listed in Table 2.1. The position of the alkyl chain is confirmed from long range correlation peaks observed between 11, 12, 3b, 5b, 13a, 9a, 14b, 8a, 10, 13 carbon atoms and protons on the aliphatic tail. The intermolecular correlations between the 3′^{1}, 3′^{2}, 3′′^{1}, 3′′^{2} and the 4, 5 ^{13}C are indicated with an asterisk. Many correlations in the dataset recorded with a long mixing time are intermolecular.

2.2.2 LGCP build up curve

To validate the interpretation of the HETCOR data shown in Figure 2.2, LGCP build up curves (Figure 2.3) were collected with the sequence of van Rossum *et al.* (Figure S2.8B).[40] Homonuclear decoupling was achieved by applying pulses at the ± LG condition during the CP contact time. The LGCP build up curves for the 4, 5 and 13a, 9a ^{13}C can be resolved in the dataset of Figure S2.3-2.4 and are plotted against mixing time from 0 to 2 ms in Figure 2.3 with a red and green trace, respectively. Heteronuclear distances between selective nuclei can be estimated from such LGCP build up curves by simulation for various ^{1}H-^{13}C distances using the SIMPSON virtual spectrometer software.[41] Both traces are in line with a simulation for a single ^{1}H-^{13}C pair of spins separated by ~3 Å, corresponding to a dipolar coupling frequency of -1.1 kHz. The relatively short intermolecular distance may indicate the parallel transfer of polarization from a proton cloud to a nearby ^{13}C nucleus. The observation that two different build up signals from nearby abundant ^{1}H nuclear species into a ^{13}C at natural abundance can be

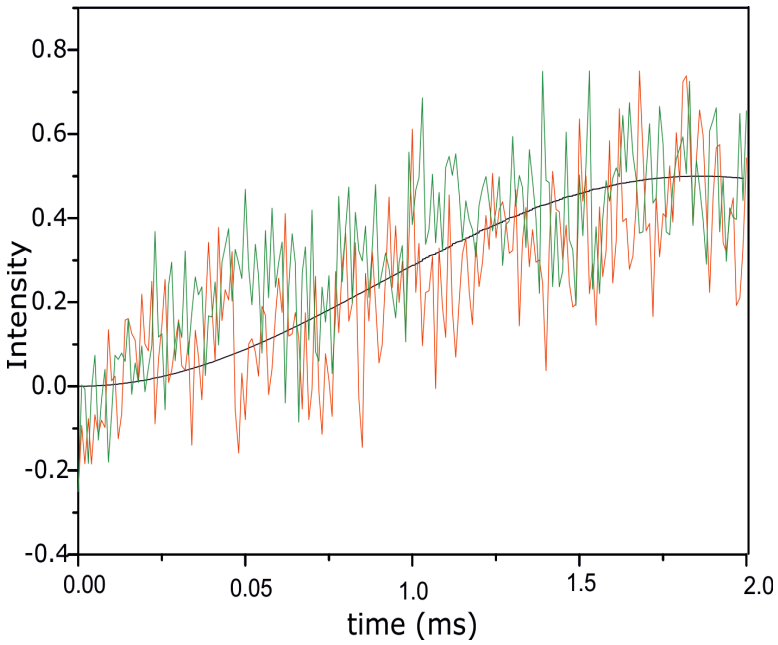

Figure 2.3 2-D LGCP build-up curves of 4/5 carbon nuclei (red) and 13a/9a carbon nuclei (green) were compared with a simulated buildup for a heteronuclear ^{1}H-^{13}C spin pair separated by 3 Å (black).

superimposed onto one another and yield similar coherent buildup transfer is intriguing. It may indicate a general property of intermolecular heteronuclear buildup in rigid systems, which can serve as a practical rule for structure determination of moderately sized molecular systems with ^{13}C at natural abundance. The 3b, 5b ^{13}C in the central part of the NDI motif correlate with the 2^{1} and 7^{1} CH_2 protons. The intramolecular distance is 4.4 Å, which is rather long. The correlation, therefore, can be intermolecular, indicative of the formation of J-aggregates with a slipped arrangement of the NDI moieties since this would position the alkyl tail above the plane of a neighbouring molecule and would imply that the correlations and buildup from protons at the alkyl chain to 13a, 9a ^{13}C are intermolecular. Similarly, the buildup of CP intensity from the alkyl CH_2 to the quaternary ^{13}C on the phenazine core can be considered intermolecular from the abundant ^{1}H nuclei on the alkyl chain. There are no intramolecular correlation signals for the 10, 13 or other aromatic protons with their quaternary neighbours. In addition, the 9 N-H was found to resonate downfield ~ 10 ppm in the homologue and there are no correlation signals in this region in the HETCOR dataset with a long mixing time as well (data not shown).

2.2.3 Cryo EM measurements

A high-resolution TEM image of the DATZnS(3′-NMe) deposited on a carbon electrode reveals a layered periodic arrangement (Figure 2.4A). Fourier transformation of the selected region indicated by a dashed square shows periodic spacings of 1.685 nm and 0.547 nm in mutually orthogonal directions (Figure 2.4B). This represents the preferred orientation, as it was difficult to find other alignments with clear reflections. The TEM data thus provide enough evidence to converge on a monoclinic packing with the molecule along the unique axis of 1.685 nm, parallel to the surface. This is in line with the head to tail molecular recognition deduced from the NMR distance constraints. The reflections cannot all be of first order, as this would lead to a density that is at least a factor two too high, depending on the number of molecules in the unit cell. Along the direction of 1.685 nm, there are two strong centrosymmetric reflections, which can be of first order since the size of the molecule along the long axis is around 1.685 nm. In addition, higher order weak reflections without any systematic absence are also observed in the same direction. Perpendicular to the direction of 1.685 nm there are series of reflection spots with a systematic absence pointing to reflection condition *h0l*: *l = 2n*. This systematic absence implies a translational component, a screw axis or glide plane, in the symmetry operations for the packing space group. The 1.24 nm reflection observed (Figure S2.5) at high magnification should be either a first order reflection with one molecule per unit cell or a second order reflection with two enantiomers per unit cell to arrive at a density around 1.67 g/cm^3 and account for the symmetry in the NMR response. Interestingly there is also a 0.74 nm reflection spot (Figure S2.5), which could be a higher order reflection of the third axis. Although at this point considering the strength of the reflection spots, other polymorphs cannot be excluded.

2.3 Discussion

2.3.1 Antiparallel lamellar packing of DATZnS(3’-NMe)

For moderately sized molecules with functionalities protruding, packing will inevitably lead to steric conflicts unless screw axes or glide planes, symmetry operations containing a translational component, are invoked that allow for an

interpenetration of parts of the structure containing symmetry-related molecules. This is the reason why by far most of the nonchiral organic packings are in the $P2_1/c$ space group, which as both a 2_1 screw axis and a c-glide plane. This implies two independent, symmetry related positons in a chiral packing with a twofold axis, or two enantiomers can be present in an equal amount to establish a racemic packing with four inequivalent sites, two from the twofold axis in the DATZnS(3'-NMe) and two from the enantiomeric pair (Figure 2.1). The monoclinic space groups with a twofold axis are $P2$, $C2$, $P2/m$, C2/m, P$2/c$, and $C2/c$. Of these, $P2$ and $P2/m$ do not have reflection conditions and can be discarded. The chiral space group $C2$ has four independent positons while only two are needed for a chiral packing. Likewise, the achiral space groups $C2/m$, and $C2/c$ have eight independent positions, while only four are needed for a racemic packing. This effectively limits the space group to $P2/c$, with unidirectional donor-on-donor and acceptor-on-acceptor columnar arrays in an extended and layered antiparallel monoclinic unit cell with a twofold axis and a glide plane (Figure 2.5).[42] The $P2/c$ space group has reflection conditions in line with the experimental diffraction pattern. The molecular arrangement was modeled in a $P2/c$ unit cell with dimensions a = 0.547 nm, b = 1.685 nm, c = 2.517 nm and $\beta = 102°$, taken from the TEM images (Figure 2.4). First, a monomer was optimized with the Dreiding force field in FORCITE and refined at the DFT level with DMol^3 to determine the atomic charges. The total charge was set to zero, and the molecule was then positioned with the C_2 molecular axis aligned onto the twofold symmetry axis in the unit cell, second setting with B-Unique, Cell1 in Materials Studio. The four symmetry operations then generate two pairs of enantiomers, and only one set of enantiomers was kept. With a density of 1.67 g/cm^3, the position along the twofold axis was varied to minimize steric hindrance. The structure was optimized with FORCITE, leading to an energy of 170.5 kcal/mol. To validate the structure, we performed an optimization without constraining the cell, which led to virtually the same result, and we performed a polymorph analysis with Materials Studio to verify the possibility of other packings with higher density and lower energy across the five most frequent space groups, which we were not able to find. The $P2/c$ has by far the highest density and lowest lattice energy among the packings with other possible space groups.

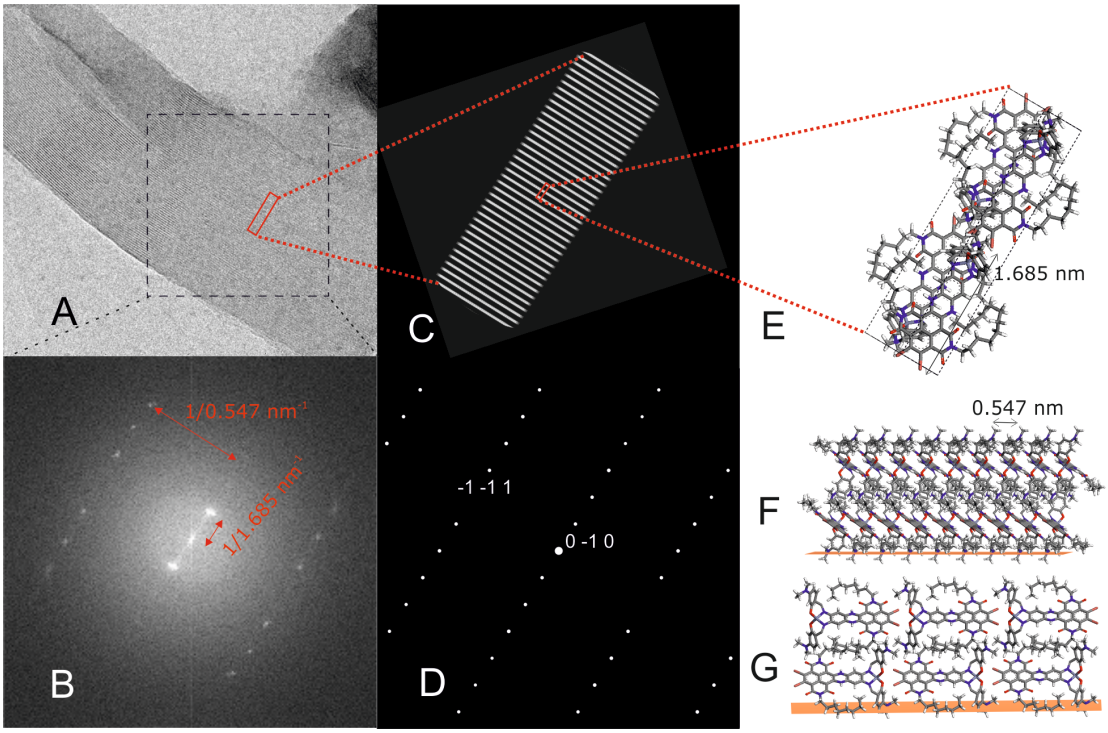

Figure 2.4 Integration of TEM and MAS NMR data to resolve the DATZnS(3′-NMe) structure. (A) TEM image of the DATZnS(3′-NMe) deposited on a carbon grid, revealing the lamellar character of the compound and (B) the Fourier transform of the selected region showing the TEM diffraction pattern with systematic absences. In (D) the simulated diffraction pattern obtained with the NMR derived geometry optimized DATZnS(3′-NMe) stacks in the *P*2/*c* space group (E) is shown. The projection of the electron density map with a 40*20*2 supercell is shown in panel (C). The orientation of the compound on the carbon grid is schematically indicated in (F) and (G).

The DATZnS(3′-NMe) forms a tightly packed J-aggregate with a distance of 0.36 nm between NDI planes. Such short distances are commonly encountered for various classes of aggregated aromatic dyes.[43-45] Strong π-π stacking interactions and aligned electric dipoles may explain why the molecule has a high density and a low energy and is virtually insoluble. The aliphatic tails are oriented in the same direction as the salphen wings and are in voids between the phenazine moieties. A tight packing with the alkyl chains folded along the phenazine bridge of a neighbouring molecule explains the observation of strong heteronuclear correlation signals between the abundant aliphatic ^{1}H and rare phenazine ^{13}C spins, with distances between 0.2 and 0.4 nm providing very effective pathways for polarization transfer (Figure 2.3). The molecular recognition that leads to the head to tail orientation and distorted octahedral surrounding of the Zn^{2+} ion puts

the 3′-NMe of a salphen at a distance of 0.32 nm from the 4, 5 ^{13}C in the NDI, which is also in quantitative agreement with the LGCP buildup kinetics data and the SIMPSON analysis shown in Figure 2.3.

For the simulation of the diffraction pattern the model was read into CrystalMaker, oriented, and projected onto the TEM diffraction pattern in SingleCrystal (Figure 2.4D). The model was oriented by performing visual matching of the simulated diffraction with the observed Fourier transform. A view direction along the 0.69, 0, 0.69 lattice vector gave the best match on an average orientation for the DATZnS(3′-NMe) on the EM grid, with the indexing of the diffraction image as indicated in Figure 2.4D. The analysis validates the systematic absence of reflections from the *c*-glide plane in the $P2/c$ space group, and shows that -1 0 1 and 1 0 -1 are quenched (Figure 2.4B). The strong 0 1 0 and 0 -1 0 are from the lamellar spacing and alternating regions of zinc salphen and NDI. The alternating electron density observed in the TEM image was reproduced from a 40*20*2 super cell constructed out of a unit cell along the surface. An electron density map was generated and then projected onto a plane with the EMAN electron microscopy processing suite, which is in correspondence with TEM image (Figure 2.4C). In the preferred orientation the DATZnS(3′-NMe) molecules are oriented parallel to the electrode surface as in Figure 2.4F. The phenazine dipoles are aligned along the surface while the NDI stacks are running at an angle of 45° with the plane of the NDI rings parallel to the surface (Figures 2.4E, F).

2.3.2 Insight into the packing

In Figure 2.5 it is shown how the molecular recognition leads to a hierarchy in the suprastructure. At the basis there is twofold C_2 symmetry of the DATZnS(3′-NMe) (Figure 2.5A). In the competition between accommodating functionalities by screw axes and glide planes, apparently, the screw axis is suppressed in favour of a twofold axis to accommodate the C_2 symmetry. This is possible because of a rich structural variability introduced with the nonplanar metal salphen that has Λ and Δ enantiomer. The structural variability allows for an overall packing in an achiral $P2/c$ space group with a racemic mixture of the two enantiomeric species, thereby circumventing the need for a screw axis in favour of a *c*-glide plane with inversion symmetry in the structure. Thus, while $P2_1/c$ is by far the most common space

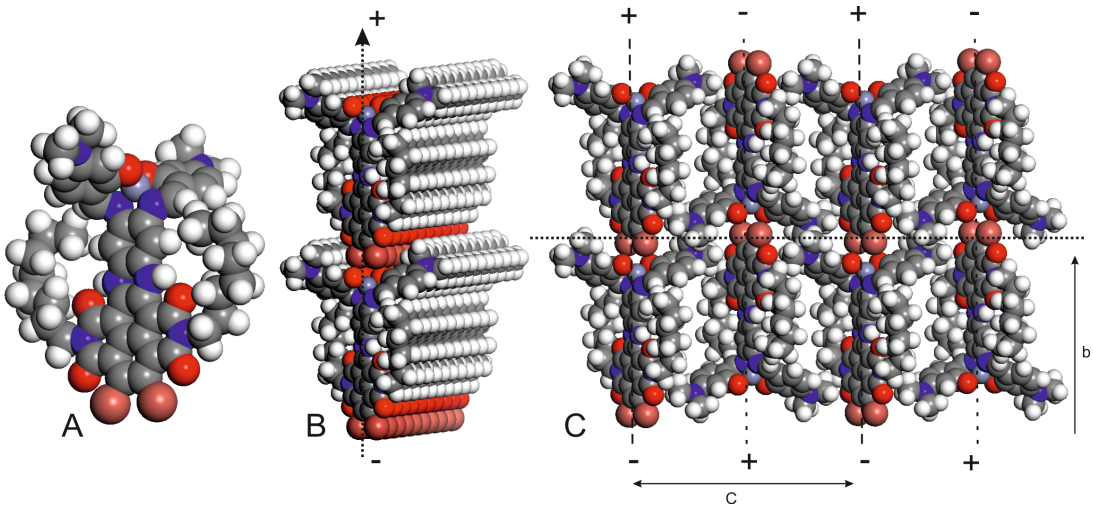

Figure 2.5 Molecular recognition for steering the packing of DATZnS(3′-NMe) starts from chiral building blocks with C_2 symmetry (A). These self-assemble into enantiomerically pure polar layers with a $P2$ surface symmetry to accommodate the twofold axis. The layers comprise arrays of aligned dipoles with a positive salphen side and negative Br side (B). Alternating layers with opposite chirality self-assemble with a *c*-glide to release steric hindrance and establish a dense packing with quenching of electric dipoles (C).

group for optically active organic species, here in this work, it is managed to steer away by molecular recognition and chemical programming of a twofold axis at the molecular level, which does not "fit" in a $P2_1/c$ framework. This is similar to the concept of an induced fit or misfit in biological samples.[15]

2.3.3 Orientation of the molecule on the surface

With the C_2 molecular symmetry preserved, the DATZnS(3′-NMe) self assembles into polar planes without inversion symmetry elements (Figure 2.5B). Here the selectivity induced by the chirality that emerges at the salphen motif is essential. Chiral expression at surfaces and planes has attracted considerable attention in recent years. Only five possible chiral space groups can exist at a surface and the DATZnS(3′-NMe) is forced into a $P2$ plane by the molecular C_2 symmetry, the molecular recognition and for energetic reasons.[46] The electric dipoles align and form extended arrays with a positive and a negative side, which may be of interest to support charge separation following light absorption in the NDI columns running perpendicular to the electric field direction in the $P2$ plane of chiral molecules (Figure 2.5B). It is easy to create chirality in a 2D system since a surface

cannot possess a center of inversion and can only maintain reflection mirror symmetry planes normal to the surface, which leads to the $P2/c$ arrangement shown in Figure 2.5C with the two enantiomeric species forming planes of alternating chirality. In the proposed 3D model the net dipole moment cancels due to the antiparallel stacking of layers. Hence, the DATZnS(3′-NMe) forms extended chiral domains arising from the planar arrangements of the individual $C2$ motifs, a concept known as organizational chirality.[46] Because of the close analogy between surfaces and planes, it is anticipated that this molecular steering concept can be further developed for the chemical design of functional electrodes. With the DATZnS(3′-NMe) forming polar layers, there is the possibility to deliver electrons at the salphen side to an electrode or tailor the template to incorporate a catalyst in a solar fuel cell device architecture. In parallel introduction of electron donating or withdrawing groups to the core of the naphthalene shifts the optical absorption, making it suitable for tuning the optoelectronic properties.[47,48]

2.4 Conclusions

The molecular structure and packing of paracrystalline DATZnS(3′-NMe) oriented on a surface grid was studied in detail in the solid state. DATZnS(3′-NMe) lamella pack in a $P2/c$ space group with alkyl chains folding along the phenazine and the zinc in a pseudo octahedral environment with adjacent bromine atoms. Symmetry and distance constraints obtained from CP/MAS NMR in association with reflections in the diffraction pattern were used to converge on a racemic packing with four independent positions starting from chiral building blocks with C_2 symmetry. The system combines a high density of 1.67 g/cm^3 with a low energy in comparison with other polymorphs. The molecular recognition and molecular symmetry are used to steer the packing and associated functional characteristics by forcing the system into a racemic packing and use a c-glide plane with inversion symmetry to release steric hindrance. The combination of MAS NMR, cryo-EM and molecular modeling with periodic boundary conditions in the form of a space group provides a promising approach that can be of use in the future to investigate structure and properties of other unlabeled moderately sized supramolecular systems.

2.5 Materials and methods

2.5.1 Sample preparation

For the purpose of this study Zinc(II) 6,6'-((1E,1'E)-((4,5-dibromo-2,7-dioctyl-1,3,6,8-tetraoxo-1,2,3,6,7,8,9,14-octahydro-[3,8] phenanthrolino [1,10-abc] phenazine-11,12-diyl) bis (azanylylidene)) bis (methanylylidene))bis(3-(dimethylamino)phenolate) (DATZnS(3'-NMe)) molecule is used (Figure 2.1).[17] The DATZnS scaffold is a hybrid material with a core expanded naphthalene diimide (cNDI) supramolecularly coupled with a zinc bis-salicyimide phenylene (salphen) moiety and can be functionalized with 3′-NMe or 2′,4′-tBu functional groups (Figure S2.2).[17] For the synthesis, anhydrous N,N-dimethylformamide (DMF) was obtained from Sigma-Aldrich and used as received. Melting points were measured using ΔT = 1 °C min^{-1} on a Stuart Scientific SMP3 melting point apparatus and are uncorrected. Infrared (IR) spectra were recorded neat using a Shimadzu FTIR-8400s spectrophotometer and wavelengths are reported in cm^{-1}. Unless stated otherwise, all reagents were used as received from commercial vendors.

Synthesis of DAT-diamine: In a small round bottom flask, 15 mL of 98% H_2SO_4 was degassed for 15 min using an N_2 stream. DATTs[49] was added as a solid (131 mg, 0.12 mmol) and the resulting turquoise solution was stirred under N_2 atmosphere for 4 days. The reaction mixture was transferred under vigorous stirring into a 1 L flask containing 500 mL of H_2O and 200 mL of dichloromethane, after which $NaHCO_3$ was added as a saturated aqueous solution until gas evolution ceased. The organic phase was separated and concentrated under vacuum. A dark blue solid (DAT-diamine) was obtained in quantitative yield (85 mg). This solid readily aggregates in solution, prohibiting recording of ^1H and ^{13}C solution NMR spectra. FTIR: 3456, 3416, 3362, 3339, 2953, 2914, 2849, 1678, 1570, 1489, 1452, 1425, 1286, 1234, 1134, 1094, 1013, 874, 812, 660 cm^{-1}. The first four frequencies are indicative of the presence of aniline like N-H stretching vibrations.

Synthesis of DATZnS(3′-NMe): DAT-diamine intermediate (142 mg, 0.18 mmol) was prepared from DATTs, was dissolved in 15 mL dry, degassed DMF under an Ar atmosphere and heated to 110 °C in the dark. In a separate flask, 4-

dimethylaminosalicylaldehyde (60 mg, 0.37 mmol) and zinc acetate dihydrate (320 mg, 1.75 mmol) were dissolved in dry, degassed DMF (5 mL) and kept under Ar. This mixture was stirred for 5 minutes and added to the hot DMF solution via a syringe. After 4 hours, the reaction mixture was cooled down to room temperature and diluted with 25 mL saturated aqueous $NaHCO_3$ solution to induce precipitation. The dark blue precipitate was collected on a filter and washed with water, ethanol and chloroform to afford (after vacuum drying) 221 mg of a dark blue solid (95 % yield from DAT-diamine). IR (ATR FTIR): 3497, 3371, 2923, 2856, 1684, 1610, 1570, 1560, 1448, 1431, 1375, 1358, 1279, 1246, 1182, 1151, 843, 669, 660, 661, 584 cm^{-1}. Mp: > 300° C

2.5.2 NMR measurements

NMR spectra with high sensitivity and high resolution were obtained by exploiting heteronuclear cross polarization (CP) along with magic angle spinning (CPMAS), in which polarization is transferred from abundant ^{1}H spins to the dilute ^{13}C nuclei, followed by the observation of the signals from the carbon. MAS NMR experiments were performed on a Bruker AV-750 spectrometer equipped with a 4 mm triple resonance MAS probe head, using a ^{13}C radio frequency of 188.6 MHz and data were collected at a sample temperature of 298 K. The ^{79}Br resonance from KBr was used to set the magic angle. A spinning frequency of 11 kHz ± 5Hz was used for the 2D ^{1}H-^{13}C heteronuclear correlation experiments. The ^{1}H spins were decoupled during acquisition using the two-pulse phase modulation TPPM scheme. Two-dimensional ^{1}H-^{13}C heteronuclear correlation data sets were obtained with the Phase Modulated Lee Goldburg (PMLG) experiment with a short CP time of 0.256 ms and a long CP time of 4 ms (Figure S2.2A). The ^{1}H chemical shift was calibrated with a HETCOR dataset collected from tyrosine.HCl salt. A Frequency-Switched Lee-Goldburg (FSLG) scale factor of 0.571 reproduces the ^{1}H chemical shifts for Tyrosine in solution. To collect the data set for the LGCP build up curves, the sequence in Figure S2.8b was used. LG conditions were applied during CP and the contact time was increased from 0.1 to 2 ms.[39] NMR data were processed using the TopSpin 3.2 software (Bruker, Billerica, MA). OriginPro 9.1 (OriginLab Corporation, Northampton, MA) was used to process the LGCP build up curves for the selected ^{13}C nuclei and to do the Fourier transformation. LGCP build up curve

simulations were performed using the open-source simulation software SIMPSON for $^{1}H–^{13}C$ spin systems with REPULSION powder averaging over a set of 66 Euler angles with 8 γ angles at 11 kHz spinning and a static field corresponding to 750 MHz for ^{1}H (S2.6).

2.5.3 Cryo-EM measurements

Samples for CryoEM were prepared by gently "crushing" the material with a small spatula onto a glass slide. It was suspended in ethanol and after settling a droplet from the upper half of the suspension containing the smaller fragments was put onto a carbon-coated grid, blotted, and dried in air. The samples were cooled down to -180˚ in the microscope and imaged with 300 kV electrons. Electron microscopy was performed with a Tecnai G2 Polara electron microscope (FEI, Hillsboro, OR) equipped with a Gatan energy filter at 115,000× magnifications (Gatan, Pleasanton, CA). Images were recorded in the zero-loss imaging mode, by using a slit-width of 20 eV, with a slow-scan CCD camera at 1 μm under focus, to have optimal phase contrast transfer at 300 kV for details with a periodicity of ≈2 nm. 3D electron density was simulated from atomic coordinates at 0.6 nm resolution by using the EMAN pdb2mrc program. The electron density map was projected onto a plane using the EMAN proc3d program to get a simulated EM image. Simulation of the TEM diffraction was performed with SingleCrystal (Crystalmaker Software Ltd, Oxford) after orienting the crystal structure in the CrystalMaker (Crystalmaker Software Ltd, Oxford) software.[50,51]

2.5.4 Structure modeling and chemical shift calculation

Computational modeling was performed with the Biovia Materials Studio Suite (Biovia, San Diego, CA). Racemic packings were obtained for different space groups. A set of unit cells with a twofold axis was selected to accommodate the C_2 symmetry. The monomer was positioned along the twofold axis in a unit cell with the parameters obtained from TEM. The monomer was shifted and rotated to minimize steric hindrance and spurious doublings were removed by hand to obtain a reasonable density. The structure was then optimized using the FORCITE module with the Dreiding force field and ESP charges calculated with DMol^3 for the molecule in its C_2 configuration. Calculations were performed with DMol^3 as

implemented in DMol[3] package. The generalized gradient approximation (GGA) with the Perdew–Burke–Ernzerhof (PBE) functional is employed. In this work, the double numerical atomic orbital augmented by a polarization p-function (DNP) is chosen as the basis file 3.5. Global orbital cutoff value is 3.9 Å.

NMR chemical shift calculations for monomers were performed by optimizing the structure using the Gaussian 03 software package (Gaussian, Inc., Wallingford, CT) with the Becke, Lee, Yang, and Parr (BLYP) exchange-correlation functional with 6-311G basis set and using the NMR module in Gaussian 03.[52]

References

(1) Cook, T. R.; Dogutan, D. K.; Reece, S. Y.; Surendranath, Y.; Teets, T. S.; Nocera, D. G. *Chemical Reviews* **2010**, *110*, 6474.

(2) Chu, S.; Majumdar, A. *Nature* **2012**, *488*, 294.

(3) Lewis, N. S.; Nocera, D. G. *Proceedings of the National Academy of Sciences* **2006**, *103*, 15729.

(4) Abbott, D. *Proceedings of the IEEE* **2010**, *98*, 42.

(5) Kutal, C. *Journal of Chemical Education* **1983**, *60*, 882.

(6) Kim, D.; Sakimoto, K. K.; Hong, D.; Yang, P. *Angewandte Chemie International Edition* **2015**, *54*, 3259.

(7) Listorti, A.; Durrant, J.; Barber, J. *Nat Mater* **2009**, *8*, 929.

(8) Wondraczek, L.; Tyystjärvi, E.; Méndez-Ramos, J.; Müller, F. A.; Zhang, Q. *Advanced Science* **2015**, *2*, n/a.

(9) Faunce, T. A.; Lubitz, W.; Rutherford, A. W.; MacFarlane, D.; Moore, G. F.; Yang, P.; Nocera, D. G.; Moore, T. A.; Gregory, D. H.; Fukuzumi, S.; Yoon, K. B.; Armstrong, F. A.; Wasielewski, M. R.; Styring, S. *Energy & Environmental Science* **2013**, *6*, 695.

(10) Gust, D.; Moore, T. A. *Science* **1989**, *244*, 35.

(11) Young, K. J.; Martini, L. A.; Milot, R. L.; Snoeberger Iii, R. C.; Batista, V. S.; Schmuttenmaer, C. A.; Crabtree, R. H.; Brudvig, G. W. *Coordination Chemistry Reviews* **2012**, *256*, 2503.

(12) Bottari, G.; Trukhina, O.; Ince, M.; Torres, T. *Coordination Chemistry Reviews* **2012**, *256*, 2453.

(13) Eisenberg, R.; Nocera, D. G. *Inorganic Chemistry* **2005**, *44*, 6799.

(14) Purchase, R. L.; de Groot, H. J. M. *Interface Focus* **2015**, *5*.

(15) Alia, A.; Buda, F.; Groot, H. J. M. d.; Matysik, J. *Annual Review of Biophysics* **2013**, *42*, 675.

(16) Purchase, R. L.; de Groot, H. J. M. *Interface Focus* **2015**, *5*, 20150014.

(17) Rombouts, J. A.; Ravensbergen, J.; Frese, R. N.; Kennis, J. T. M.; Ehlers, A. W.; Slootweg, J. C.; Ruijter, E.; Lammertsma, K.; Orru, R. V. A. *Chemistry – A European Journal* **2014**, *20*, 10285.

(18) Lin, C.-C.; Velusamy, M.; Chou, H.-H.; Lin, J. T.; Chou, P.-T. *Tetrahedron* **2010**, *66*, 8629.

(19) Grunder, S.; Muñoz Torres, D.; Marquardt, C.; Błaszczyk, A.; Krupke, R.; Mayor, M. *European Journal of Organic Chemistry* **2011**, *2011*, 478.

(20) Hendsbee, A. D.; McAfee, S. M.; Sun, J.-P.; McCormick, T. M.; Hill, I. G.; Welch, G. C. *Journal of Materials Chemistry C* **2015**, *3*, 8904.

(21) Shao, H.; Parquette, J. R. *Chemical Communications* **2010**, *46*, 4285.

(22) Whiteoak, C. J.; Salassa, G.; Kleij, A. W. *Chemical Society Reviews* **2012**, *41*, 622.

(23) Clarke, R. M.; Storr, T. *Dalton Transactions* **2014**, *43*, 9380.

(24) Wu, S.; Zhong, F.; Zhao, J.; Guo, S.; Yang, W.; Fyles, T. *The Journal of Physical Chemistry A* **2015**, *119*, 4787.

(25) Bhosale, S. V.; Jani, C. H.; Langford, S. J. *Chemical Society Reviews* **2008**, *37*, 331.

(26) Paulo, P. M. R.; Costa, S. M. B. *Journal of Photochemistry and Photobiology A: Chemistry* **2012**, *234*, 66.

(27) Aratani, N.; Kim, D.; Osuka, A. *Accounts of Chemical Research* **2009**, *42*, 1922.

(28) Beletskaya, I.; Tyurin, V. S.; Tsivadze, A. Y.; Guilard, R.; Stern, C. *Chemical Reviews* **2009**, *109*, 1659.

(29) Han, D.; Du, J.; Kobayashi, T.; Miyatake, T.; Tamiaki, H.; Li, Y.; Leng, Y. *The Journal of Physical Chemistry B* **2015**, *119*, 12265.

(30) Kim, H.; Li, H.; Maresca, J. A.; Bryant, D. A.; Savikhin, S. *Biophysical Journal* **2007**, *93*, 192.

(31) Fujita, T.; Huh, J.; Saikin, S. K.; Brookes, J. C.; Aspuru-Guzik, A. *Photosynthesis Research* **2014**, *120*, 273.

(32) Pšenčík, J.; Collins, A. M.; Liljeroos, L.; Torkkeli, M.; Laurinmäki, P.; Ansink, H. M.; Ikonen, T. P.; Serimaa, R. E.; Blankenship, R. E.; Tuma, R.; Butcher, S. J. *Journal of Bacteriology* **2009**, *191*, 6701.

(33) Pšenčík, J.; Arellano, J. B.; Ikonen, T. P.; Borrego, C. M.; Laurinmäki, P. A.; Butcher, S. J.; Serimaa, R. E.; Tuma, R. *Biophysical Journal* **2006**, *91*, 1433.

(34) Chakrabarty, R.; Mukherjee, P. S.; Stang, P. J. *Chemical reviews* **2011**, *111*, 6810.

(35) Ganapathy, S.; Oostergetel, G. T.; Wawrzyniak, P. K.; Reus, M.; Gomez Maqueo Chew, A.; Buda, F.; Boekema, E. J.; Bryant, D. A.; Holzwarth, A. R.; de Groot, H. J. M. *Proceedings of the National Academy of Sciences* **2009**, *106*, 8525.

(36) Baias, M.; Dumez, J.-N.; Svensson, P. H.; Schantz, S.; Day, G. M.; Emsley, L. *Journal of the American Chemical Society* **2013**, *135*, 17501.

(37) Blümich, B.; Hagemeyer, A.; Schaefer, D.; Schmidt-Rohr, K.; Spiess, H. W. *Advanced Materials* **1990**, *2*, 72.

(38) Kaźmierski, S.; Pawlak, T.; Jeziorna, A.; Potrzebowski, M. J. *Polymers for Advanced Technologies* **2016**, n/a.

(39) van Rossum, B. J.; de Groot, C. P.; Ladizhansky, V.; Vega, S.; de Groot, H. J. M. *Journal of the American Chemical Society* **2000**, *122*, 3465.

(40) Ladizhansky, V.; Vega, S. *Journal of the American Chemical Society* **2000**, *122*, 3465.

(41) Bak, M.; Rasmussen, J. T.; Nielsen, N. C. *Journal of Magnetic Resonance* **2000**, *147*, 296.

(42) Jin, S.; Ding, X.; Feng, X.; Supur, M.; Furukawa, K.; Takahashi, S.; Addicoat, M.; El-Khouly, M. E.; Nakamura, T.; Irle, S.; Fukuzumi, S.; Nagai, A.; Jiang, D. *Angewandte Chemie International Edition* **2013**, *52*, 2017.

(43) Würthner, F.; Kaiser, T. E.; Saha-Möller, C. R. *Angewandte Chemie International Edition* **2011**, *50*, 3376.

(44) Prokhorov, V. V.; Perelygina, O. M.; Pozin, S. I.; Mal'tsev, E. I.; Vannikov, A. V. *The Journal of Physical Chemistry B* **2015**, *119*, 15046.

(45) Wang, Y. J.; Li, Z.; Tong, J.; Shen, X. Y.; Qin, A.; Sun, J. Z.; Tang, B. Z. *Journal of Materials Chemistry C* **2015**, *3*, 3559.

(46) Barlow, S. M.; Raval, R. *Surface Science Reports* **2003**, *50*, 201.

(47) Sakai, N.; Mareda, J.; Vauthey, E.; Matile, S. *Chemical Communications* **2010**, *46*, 4225.

(48) Etheridge, F. S.; Fernando, R.; Golen, J. A.; Rheingold, A. L.; Sauve, G. *RSC Advances* **2015**, *5*, 46534.

(49) Banerji, N.; Bhosale, S. V.; Petkova, I.; Langford, S. J.; Vauthey, E. *Physical Chemistry Chemical Physics* **2011**, *13*, 1019.

(50) Yin, Y. W. *Journal of the American Chemical Society* **2004**, *126*, 14996.

(51) Kohn, S. C. *Terra Nova* **1995**, *7*, 554.

(52) Frisch, M. J.; Trucks, G. W.; Schlegel, H. B.; Scuseria, G. E.; Robb, M. A.; Cheeseman, J. R.; Scalmani, G.; Barone, V.; Mennucci, B.; Petersson, G. A.; Nakatsuji, H.; Caricato, M.; Li, X.; Hratchian, H. P.; Izmaylov, A. F.; Bloino, J.; Zheng, G.; Sonnenberg, J. L.; Hada, M.; Ehara, M.; Toyota, K.; Fukuda, R.; Hasegawa, J.; Ishida, M.; Nakajima, T.; Honda, Y.; Kitao, O.; Nakai, H.; Vreven, T.; Montgomery Jr., J. A.; Peralta, J. E.; Ogliaro, F.; Bearpark, M. J.; Heyd, J.; Brothers, E. N.; Kudin, K. N.; Staroverov, V. N.; Kobayashi, R.; Normand, J.; Raghavachari, K.; Rendell, A. P.; Burant, J. C.; Iyengar, S. S.; Tomasi, J.; Cossi, M.; Rega, N.; Millam, N. J.; Klene, M.; Knox, J. E.; Cross, J. B.; Bakken, V.; Adamo, C.; Jaramillo, J.; Gomperts, R.; Stratmann, R. E.; Yazyev, O.; Austin, A. J.; Cammi, R.; Pomelli, C.; Ochterski, J. W.; Martin, R. L.; Morokuma, K.; Zakrzewski, V. G.; Voth, G. A.; Salvador, P.; Dannenberg, J. J.; Dapprich, S.; Daniels, A. D.; Farkas, Ö.; Foresman, J. B.; Ortiz, J. V.; Cioslowski, J.; Fox, D. J.; Gaussian, Inc.: Wallingford, CT, USA, 2009.

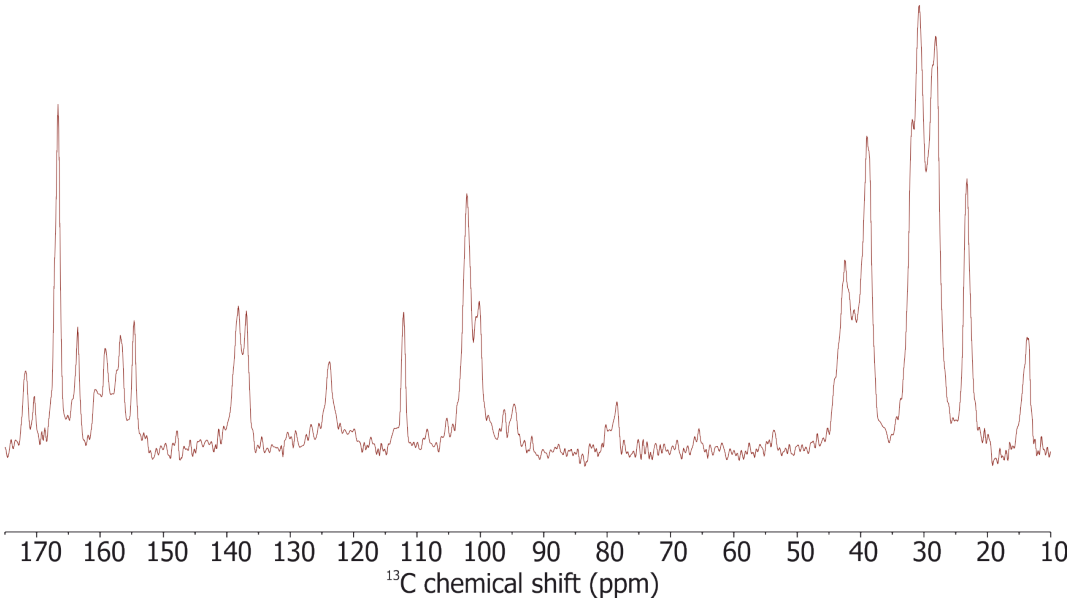

Figure S2.1 1D ^{13}C CP-MAS spectrum of DATZnS(3′-NMe). The data were collected in 3092 scans with a MAS rotation frequency of 11 kHz. Spinning side bands were identified by collecting the spectrum at different spinning frequency.

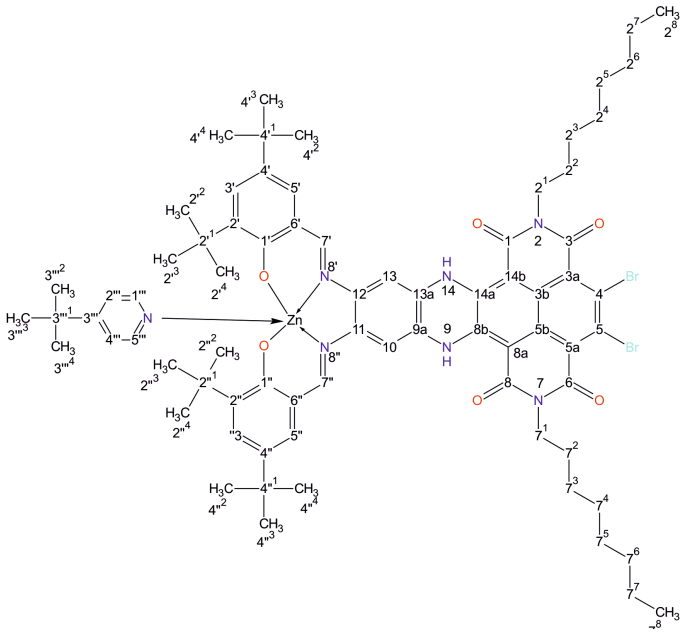

Figure S2.2 Structure of DATZnSTP homologue used for the solution state NMR assignment. Chemical shifts of corresponding carbon atoms are explained in Table 2.2.

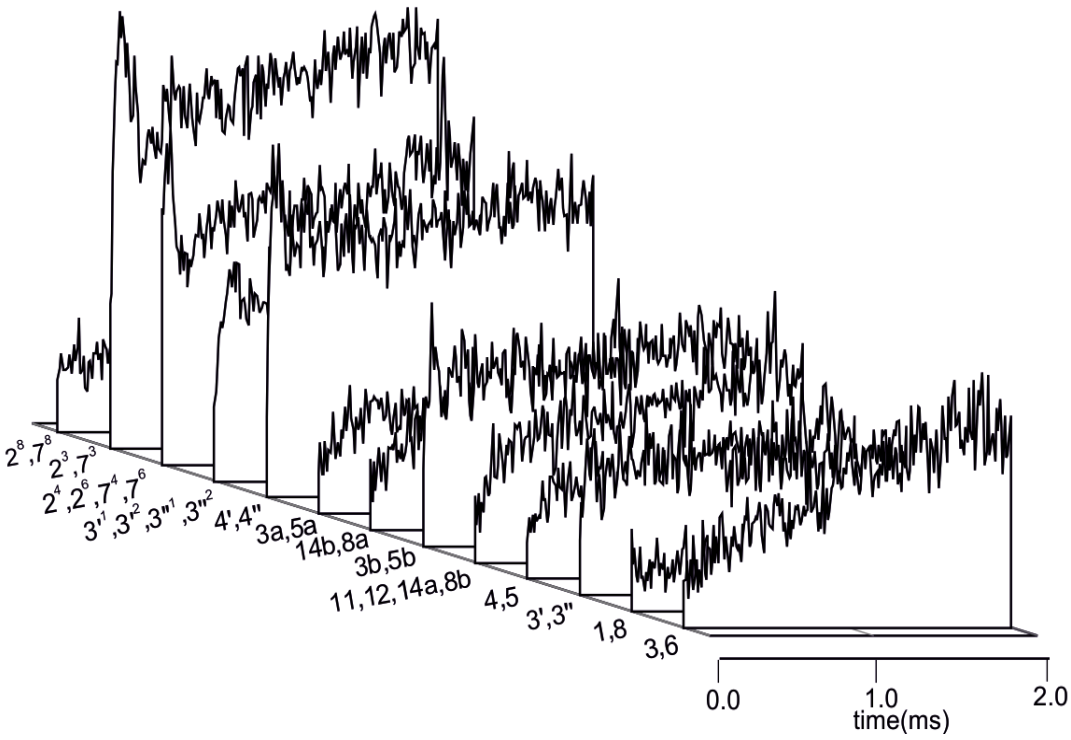

Figure S2.3 LGCP build curve plotted for selected ^{13}C nuclei.

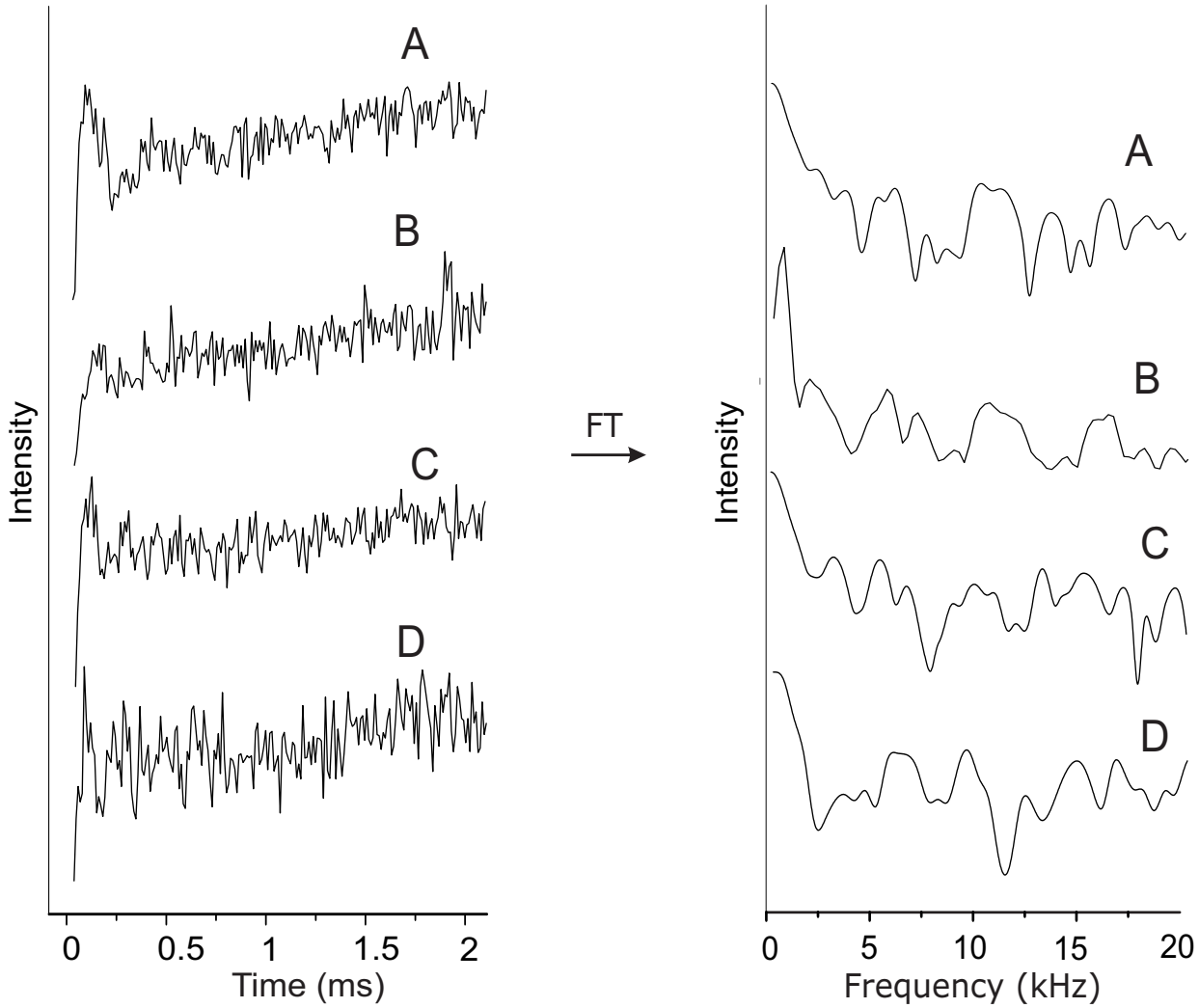

Figure S2.4 LGCP build up curve and its Fourier transform of (A) 2^3, 7^3 (B) $3'^1$, $3'^2$,$3''^1$, $3''^2$ (C) 4′, 4′′and (D) 5′, 5′′ ^{13}C nuclei. Initial sharp rise in the LGCP build up curve is due to the directly attached proton on the carbon atom. This validated the assignment of these chemical shifts to proton attached carbon atoms.

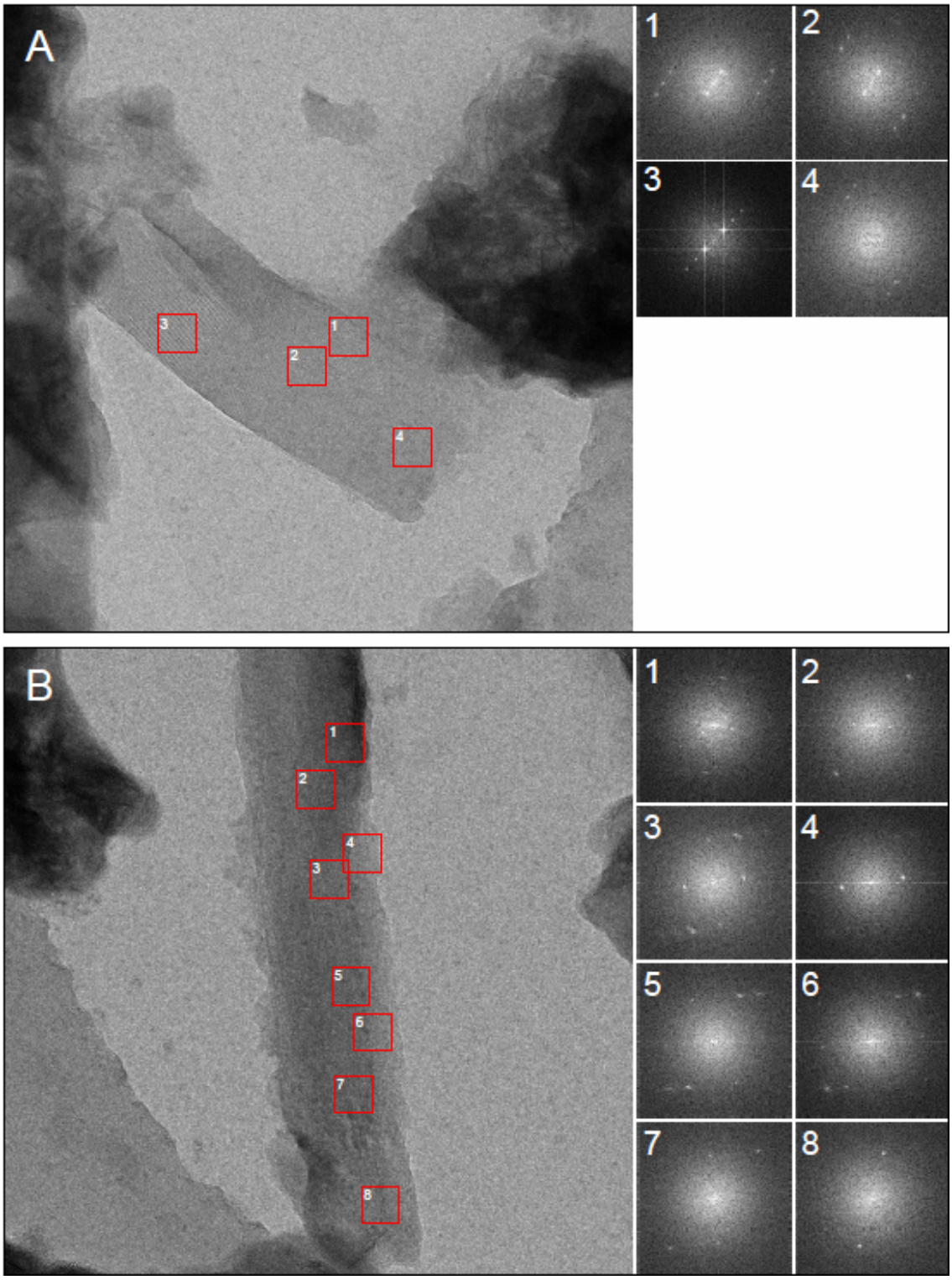

Figure S2.5 TEM image in two different orientation (A) and (B) and its Fourier transforms of selected regions showing multiple reflection spots, which are of higher order diffraction.

S2.6 Input file used for SIMPSON simulation

```
spinsys {
 channels 1H 13C
        nuclei 1H  13C
        dipole 1 2 -1118.9  0 0 0
}
par {
 method        direct
        start_operator  Inz-I2z
        detect_operator I2p
        crystal_file    rep66
        spin_rate       11000
        np              512
        gamma_angles    8
        sw              1000000
 variable    tsw 1.0e6/sw
}
proc pulseq {  } {
 global par
 pulseid 5 50000 y 0 0
 acq_block {
  pulse $par(tsw) 50000 x 40000 x
        }
}
proc pulseq_lg {} {
        global par
        set effH 50000
 set taup [expr 54.74/90.0*5]
 pulseid $taup 50000 y 0 0
 set offset [expr $effH/sqrt(3.0)]
        set rfH [expr $effH/sqrt(1.5)]
 offset $offset 0
 acq_block {
  pulse $par(tsw) $rfH x 40000 x
        }
}
proc main {} {
 global par
        set f [fsimpson]
        fsave $f $par(name).fid -binary
 set par(pulse_sequence) pulseq_lg
 set f [fsimpson]
        fsave $f $par(name)_lg.fid -xreim
}
```

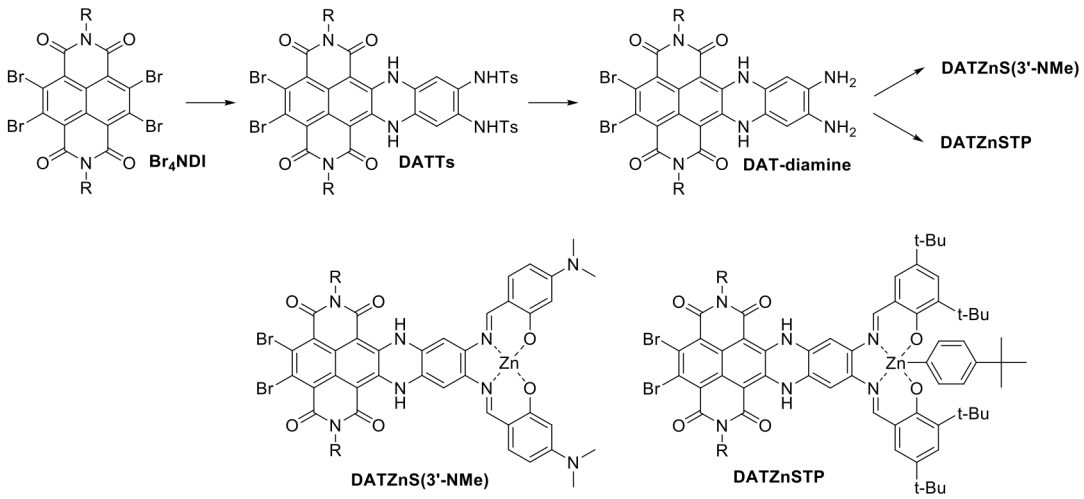

Figure S2.7 Overview of synthetic strategy towards DATZnS-dyads. R = ^{n}octyl.

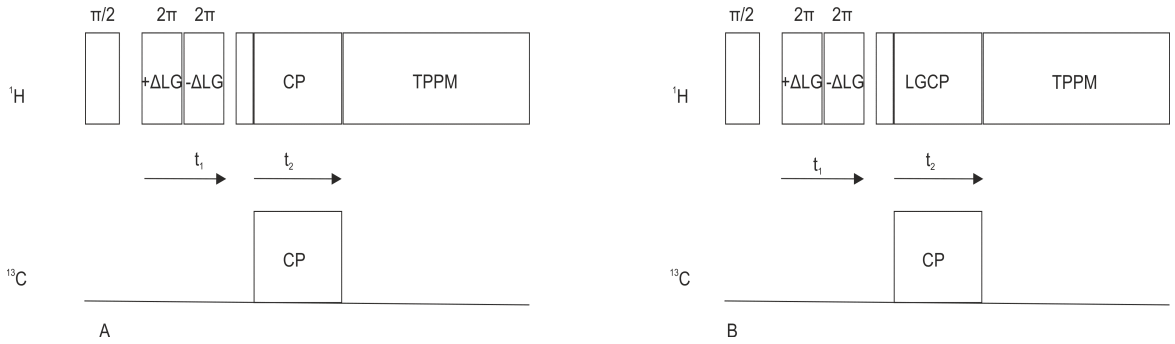

Figure S2.8 Pulse sequence used for (A) ^{1}H-^{13}C HETCOR experiment (B) for LGCP build up curve experiment.